Nanoscale

PAPER

View Article Online
View Journal | View Issue

Cite this: *Nanoscale*, 2016, **8**, 19714

The origin of facet selectivity and alignment in anatase TiO_2 nanoparticles in electrolyte solutions: implications for oriented attachment in metal oxides†

M. L. Sushko* and K. M. Rosso

Received 1st September 2016,
Accepted 4th November 2016

DOI: 10.1039/c6nr06953c

www.rsc.org/nanoscale

Oriented attachment (OA) is an important nonclassical pathway for crystal growth from solution, occurring by the self-assembly of nanoparticles and often leading to highly organized three-dimensional crystal morphologies. The forces that drive nanocrystal reorientation for face-selective attachment and exclude improperly aligned particles have remained unknown. Here we report evidence at the microscopic level that ion correlation forces arising from dynamically interacting electrical double layers are responsible for face-selective attraction and particle rotation into lattice co-alignment as particles interact at long range. Atomic-to-mesoscale simulations developed and performed for the archetype OA system of anatase TiO_2 nanoparticles in aqueous HCl solutions show that face-selective attraction from ion correlation forces outcompetes electrostatic repulsion at several nanometers apart, drawing particle face pairs into a metastable solvent-separated captured state. The analysis of the facet and pH dependence of interparticle interactions is in quantitative agreement with the observed decreasing frequency of attachment between the (112), (001), and (101) face pairs, revealing an adhesion barrier that is largely due to steric hydration forces from structured intervening solvents. This finding helps open new avenues for controlling crystal growth pathways leading to highly ordered three-dimensional nanomaterials.

Introduction

Understanding the fundamental principles of crystal growth is central for the controlled synthesis of nanostructured materials with well-defined architectures and properties. Crystal growth through ion-by-ion addition is historically well established and explored. However, conditions and underlying processes that instead lead to growth through the addition of clusters or nanoparticles are much less understood. The so-called particle-based crystallization pathways are relatively newly recognized. Oriented attachment (OA) is a prime example, where larger crystals have been observed to grow principally by the self-assembly of smaller ones, which align and attach repeatedly along certain crystallographic directions. OA is unique and important in that it produces crystal morphologies that are based hierarchically on the characteristics of its nanocrystal building blocks. It has been phenomenologically documented across a diverse range of materials, within both geological environments and under controlled synthesis conditions.[1–10] In materials design, OA holds promise for the synthesis of complex three-dimensional architectures with tailored properties through control of nanocrystal morphology and solution conditions that promote face-selective attachment.

Despite its widespread significance, the chemical and physical bases for OA have remained unknown. The relevant chemical dynamics at particle–solution interfaces that produce the forces that attract, align, and attach specific crystal faces to each other are poorly characterized. *In situ* transmission electron microscopy (TEM) studies have shown that the attracted nanocrystals sample relative orientations while in a long-lived solvent-separated state at nanometer distances, possibly maintained by interparticle osmotic pressure, yet conceptually within the range of several interparticle forces that favor crystallographic alignment.[3,11,12] Systematic experimental studies have shown that OA is highly sensitive to the properties of aqueous solutions, in that even small changes in solution pH or ionic strength may disrupt the mode of nanoparticle assembly from OA to random aggregation.[4,13,14] The collective findings hint at the essential role of ion distributions in the electrical double layer (EDL) at nanocrystal–solution interfaces, which underlie both the osmotic pressure and, in principle, a facet-dependent organizing force out several nanometers from

---

Physical Sciences Division, Pacific Northwest National Laboratory, Richland, WA, USA. E-mail: maria.sushko@pnnl.gov

† Electronic supplementary information (ESI) available: Computational details. See DOI: 10.1039/c6nr06953c

charged crystal surfaces.[15,16] The forces governing face-selective assembly may involve a delicate balance of solvent and ion mediated interactions at such distances between nanoparticles.

A number of theoretical studies have aimed at understanding the driving forces of OA, but the relevant length and time scales are difficult to fully encompass. Previous molecular dynamics studies addressed either direct interactions between nanoparticles in contact,[17–19] or the final stages of the nanoparticle approach and adhesion in a vacuum and in the presence of water vapor.[20–22] At coarser length scales, mean-field theories of colloidal forces such as that by Derjaguin, Landau, Verwey, and Overbeek (DLVO)[23–25] have also been used to describe interparticle interactions. However, this approach treats nanoparticles as uniformly charged dielectric spheres and thus lacks clearly important details underpinning OA such as the non-uniform distribution of charged groups and charge compensating ions at various exposed nanocrystal faces. In the DLVO approach electrolyte solutions are also oversimplified as a uniform dielectric medium with a Boltzmann distribution of ions at charged surfaces. While this theory can be adequate for describing average interparticle interactions at separations exceeding 8 nm, it is not suitable at a closer range where the direction-specific forces on which OA is based operate. Nor is DLVO suitable for comprehensively treating the range of solution compositions observed for OA, in many cases incorrectly predicting the sign of the total force.[26] Addressing this nanometer-scale separation regime is key to understanding OA because it defines the encounter frequency of particles properly aligned and thereby capable of successful attachment. But this regime is also least well understood because it lies at particle separations too small for DLVO theory yet too large for access by traditional atomistic molecular dynamics simulations.

Here we report evidence for the key role of face-specific ion correlation forces at nanocrystal surfaces as the basis for OA, using an atomistic model that is specifically developed to address the microscopic physics of particle–particle interactions and the chemical dynamics of interacting EDL's approaching from several nanometers. Conceptually a wide range of interparticle forces are in play, both static and dynamic in origin. At separations larger than approximately two Debye lengths, while electrostatic forces make the main repulsive contribution, attractive ion-correlation forces and static (zero frequency) particle–particle van der Waals interactions could dominate and draw particles into a close range. A further prospect of attraction through ion correlation arises from the diffuse layer of mobile counterions in the EDL at the particle–solution interfaces, which is highly polarizable, and thus at distances at which these diffuse layers interact they can couple attractively through dispersion. In a close range, while solvent-separated but net attraction persists, forces prospectively acting to align particles along specific crystallographic directions include low and high-frequency particle–particle van der Waals interactions, ion-surface dispersion interactions, and ion-correlation forces.[27] Particles can thereby be captured into a minimum on the force curve where the energy barrier to adhesion is the lowest when proper alignment is achieved. The purpose of the present study is to rigorously evaluate the balance of forces across this regime for explicitly represented crystal faces using a model encompassing the interfacial structure, the quantum and atomistic statistical mechanics, and the complexity of solution composition effects (electrolyte type, concentration, pH).

Results

We developed atomistic simulations based on classical density functional theory coupled with the Lifshitz theory of van der Waals forces to describe all relevant static and dynamical microscopic interactions between the particles in the solvent-separated state (see the ESI† for details). We apply the model to anatase TiO_2 nanocrystals, the archetypal OA system observed to self-assemble in acidic aqueous solution at elevated temperatures.[4,14] The model includes an atomic description of specific low-index faces, pH-dependent surface charge, microscopic ion–water hydration interactions, ion-surface van der Waals and image interactions, mesoscopic interactions arising from density and charge density fluctuations in the electrolyte solution (excluded volume and ion correlation interactions), Coulomb interactions and macroscopic particle–particle van der Waals interactions, that account for ion screening of the static van der Waals contribution. The model does not rely on fitted parameters, and was tested against the experimental data for ion activity[28] in the bulk solutions of 1 : 1, 2 : 1 and 3 : 1 electrolytes in the 0–2 M concentration range, and against *ab initio*[29] and distributed multipoles[30] molecular dynamics data on specific ion adsorption at the air/water interface, Monte Carlo[31] and molecular dynamics[32] data of the water structure at solid surfaces and against the experimental data[33] on the ionic atmosphere around biomolecules.[31,33,34] In the current formulation the model does not treat the chemical reactivity of particle surfaces, which are clearly important in the close range during adhesion,[21] which limits its applicability to separations above approximately 0.5 nm. Overall, however, the approach provides one possible basis for linking the solvent-separated regime to the chemical process of adhesion, for example by coupling to reactive molecular dynamics simulations developed in ref. 20 and 21, for a comprehensive statistical mechanical model of OA.

For anatase, the high frequency dielectric tensor is isotropic,[35] ruling out the possibility that high-frequency van der Waals interactions lead to face dependence. Ion-correlation forces, which are sensitive to the total charge density and to the arrangement of discrete charges on the interacting surfaces, will display face dependence if the interacting surfaces are charged.[15,16] When immersed in aqueous solution, metal oxides are characteristically reactive with water and develop a net surface charge through the protonation/hydroxylation of surface oxygen groups and/or partial adsorption/dissolution of metal cations.[36] Such chemical modifications of oxide surfaces can be controlled by varying the pH and electrolyte type and concentration. Because detailed experimental data are available on the pH dependence of the frequency of anatase nanoparticle OA in deionized water,[14,37] we focused our model specifically on this system, studying the interactions between the low-index faces of anatase in pure water and also with various concentrations of HCl to simulate the effects of pH. In this regard, our simulations are unique in that they are the first to closely mimic the experimental conditions under which anatase OA has been observed.[14]

We considered interactions between the pairs of (112), (001) and (101) anatase faces in aqueous solution, which have been experimentally observed to undergo OA most frequently, occasionally and rarely, respectively.[14] Each anatase face has a distinct arrangement of surface oxygens as shown in Fig. 1. Surface oxygens form an oblique lattice on (112), a square lattice with a unit cell edge of 0.3785 nm on (001), and a centered rectangular lattice with a 1.0240 nm × 0.3785 nm unit cell on the (101) surface. Depending on the pH, a fraction of surface oxygens on the anatase faces acquires either a positive or negative charge through protonation/hydroxylation, yielding a net charge on the face; the average point of zero net charge of anatase nanoparticles is at a pH of approximately 5.3.[38] The corresponding surface charge density depends on the pH, and also on the concentration of the electrolyte in solution and the nanoparticle size.[38] We use the experimental data for the surface charge density of anatase nanoparticles[38] and assume that charged groups are evenly distributed over the oxygen sublattice. For example, at pH 3 the experimental surface charge density is 0.15 C m^{-2} and the protonated oxygen sublattice on the (112) face will then adopt a hexagonal supercell as shown in the inset in Fig. 4. The approximation of evenly spaced discrete charges is based on the considerations of minimizing the Coulomb repulsion between like-charges, making the evenly spaced charge arrangement most energetically favorable. This approximation is likely to break down at the corners or around the defect sites, where significant variations in electrostatic potential compared to that of a plane surface can be expected.[39] Therefore the results presented here are for the interactions between the flat regions of anatase faces.

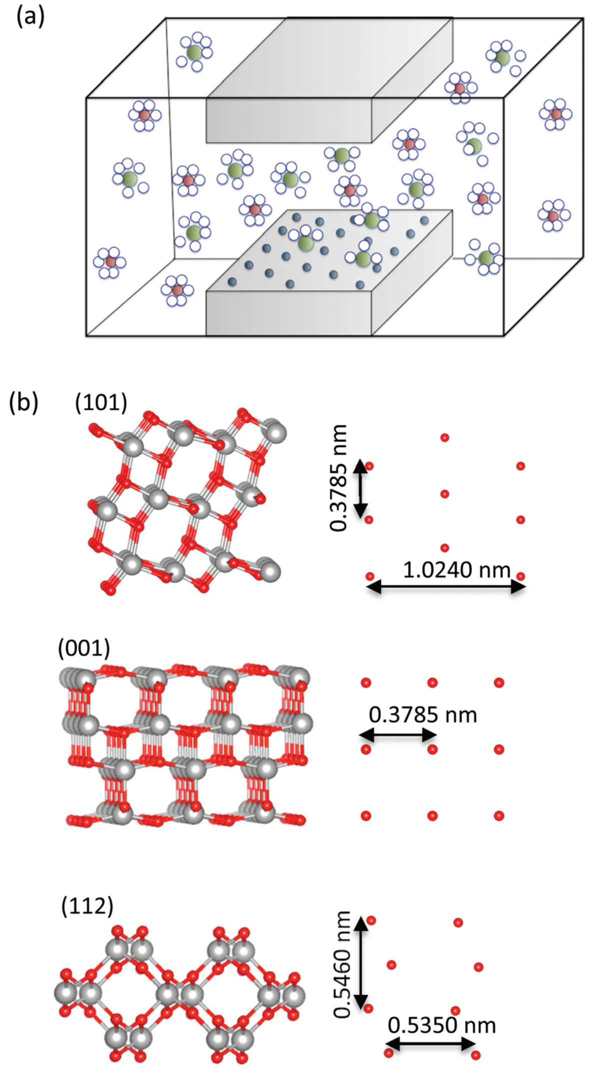

Fig. 1 The general set-up of the simulation cell (a); structures of the (101), (001) and (112) anatase surfaces adopted from previous work for our simulations, with a top view of the oxygen sublattice on each facet (b). Counterions in (a) are shown as green spheres, co-ions as red spheres, surface charges as blue spheres and water molecules as white spheres. An explicit water model was used throughout (see the ESI† for details), but only water molecules in the first ion hydration shells are represented, for clarity. In (b) Ti and O are shown as gray and red spheres, respectively.

To determine the main driving forces responsible for face specificity in the solvent-separated state we analyzed the relative contributions of attractive forces between three pairs of anatase faces at 2 nm separation in the pH range 1.2–4 (Fig. 2). Simulations show that at pH 1.2–2.1, corresponding to the concentrations of HCl in the 0.13–0.01 M range, the zero-frequency van der Waals interactions are almost fully screened and the high-frequency van der Waals forces are comparable to ion-correlation forces for all pairs of anatase faces studied. This points to a low probability of face specific interactions at extremely low pH, in good agreement with experimental observations. The balance of face-specific and isotropic attractive interactions changes in the intermediate pH range of 2.1–3.5, corresponding to the HCl concentrations of 10.0–0.316 mM. In this regime, ion-correlation forces, which are very sensitive to the distribution of discrete charges on the interacting surfaces, become almost zero for the interactions between the (101) faces and dominate attractive interactions for the pairs of the (112) and (001) faces (Fig. 2). Ion-correlation forces for the (112) and (001) faces are comparable because the spacing between the neighboring charges on both surfaces is similar (Fig. 1). Therefore, based on the analysis of attractive forces at 2 nm separation alone the probability of particle capture along the (112) and (001) faces would be similar and much higher than that along the (101) faces, under these intermediate pH conditions.

To further delineate between the probability for particle capture along the (112) and (001) faces we considered the

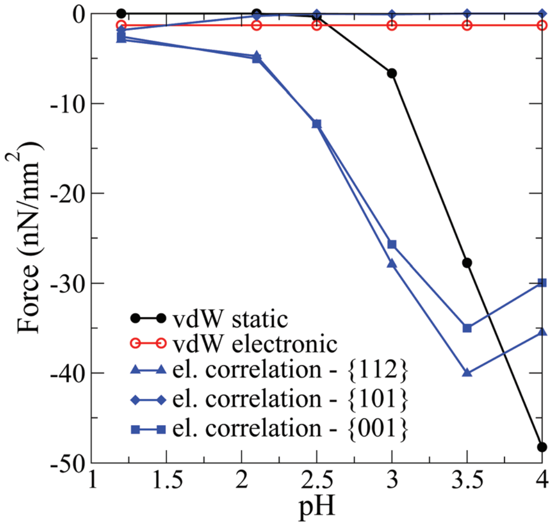

Fig. 2 pH dependence of attractive interactions between anatase TiO_2 nanoparticles at 2 nm separation. Midplane ion correlation forces are shown as blue lines, zero-frequency (static) van der Waals forces as the black line and the high frequency van der Waals forces as the red line. Ion correlation forces between two (112), two (001) and two (101) facets are shown as triangles, squares and diamonds, respectively.

details of the distance dependence of the disjoining pressure between two surfaces at pH 3 (Fig. 3). Simulations revealed the qualitative and quantitative differences in pressure–distance curves for the pairs of anatase faces studied. For the (101) surfaces the total pressure is weakly repulsive for 1.5–6 nm separations and weakly attractive with van der Waals forces dominating the attractive interactions for separations smaller than 1.5 nm. For the (112) faces the total pressure exhibits two minima: a deep minimum at 0.8 nm and a shallow secondary minimum at 1.9 nm separation between the surfaces. The main attractive contributions responsible for the primary minimum are particle–particle zero frequency van der Waals interactions and ion-surface van der Waals interactions, while the secondary minimum is due to ion correlation forces (Fig. 3b). In contrast, for the (001) surfaces there is no secondary minimum on the disjoining pressure curve. The primary minimum is located at 1.0 nm separation and is deeper than that for the (112) faces (Fig. 3c).

This deep primary minimum, corresponding to an attractive pressure of -27.0 nN nm^{-2}, is followed by an even higher barrier of 35.6 nN nm^{-2} at 0.75 nm (Fig. 3c). This energy barrier will prevent nanoparticle attachment along the (001) faces, leaving them trapped in the solvent-separated capture minimum. Such nanoparticle trapping, or capture without attachment, was observed in the *in situ* TEM experiments for iron oxyhydroxide ferrihydrite in acidic aqueous media.[11] Ferrihydrite nanoparticles were often observed to approach and persist in a solvent-separated state misaligned for several seconds, before pivoting to the side and ultimately attaching along a different face.

Our modeling findings are thus consistent with the experimental observations of the most probable attachment along (112), occasional attachment along (001) and rare attachment along (101) at pH 3.[14] More generally, they explain the driving forces for particle capture, the origin of face selectivity and alignment forces in the solvent-separated state, and barriers to attachment. In particular, the simulations revealed that the main attractive contributions to the interactions between nanoparticles are ion correlation forces, with a typical range of 0.5–6 nm, static van der Waals interactions between the anatase particles across aqueous solution with the range of 0.5–10 nm for low concentration electrolytes and 0.5–2.5 nm for electrolyte concentrations above 1 mM, and short-range ion-surface dispersion interactions significant in the 0.75–1.5 nm range of interparticle distances.

Although a comprehensive theoretical model for OA, including chemical reactive processes in a short range such as bond-breaking and interparticle attachment,[20,21] has yet to be developed, a general physical picture can now be proposed. Based on our simulations and the extensive experimental work[15] on the forces between two flat surfaces in electrolyte solutions at distances closer than can be accurately treated by mean-field theories of colloidal forces, interactions acting between two particles can be divided into three groups according to their range (Fig. 3d):

(1) *Capture minimum*: Attractive ion-correlation forces and particle–particle van der Waals interactions here dominate over repulsive electrostatic forces and give rise to a net minimum on the force curve for specific faces and conditions. This attraction increases with surface charge density and valency of the counterions,[27] which explains the experimentally observed sensitivity of the OA process to bulk solvent properties, such as pH or electrolyte concentration and chemistry.[3,13,26,40,41] In this regime, based on experimental observation[3] the net forces already display a dependence on the face-specific interfacial structure and are capable of rotating mis-aligned particles into mutual orientation. Weaker hydration and ion-surface interactions, that encompass repulsive image forces and attractive ion–mineral dispersion interactions, give rise to specific ion effects by influencing the fine details of ion distribution and, therefore, affecting the ion-correlation force.

(2) *Adhesion barrier*: In the regime when particles are separated by 3–6 solvent layers, repulsive forces are dominated by steric hydration, and monotonically repulsive forces due to the adsorbed protruding counterions causing a shift in the outer Helmholtz plane of the EDL.[15] At 0.5–1.5 nm separations while such ions are concentrated into the gap between the nanoparticles, the energy gain to hydrate these ions drives water into this region. Water structuring and associated depolarization provide a mechanism for accommodating a high concentration of water molecules in the gap between the nanoparticles as dictated by ion and surface hydration. However, the resulting loss in water entropy creates in effect an osmotic repulsive force between the interacting faces.[42,43] These forces, predominantly arising from the structure and properties of a confined solvent, collectively create an energy barrier that maintains particle separation at distances beyond the range of chemical forces responsible for adhesion.

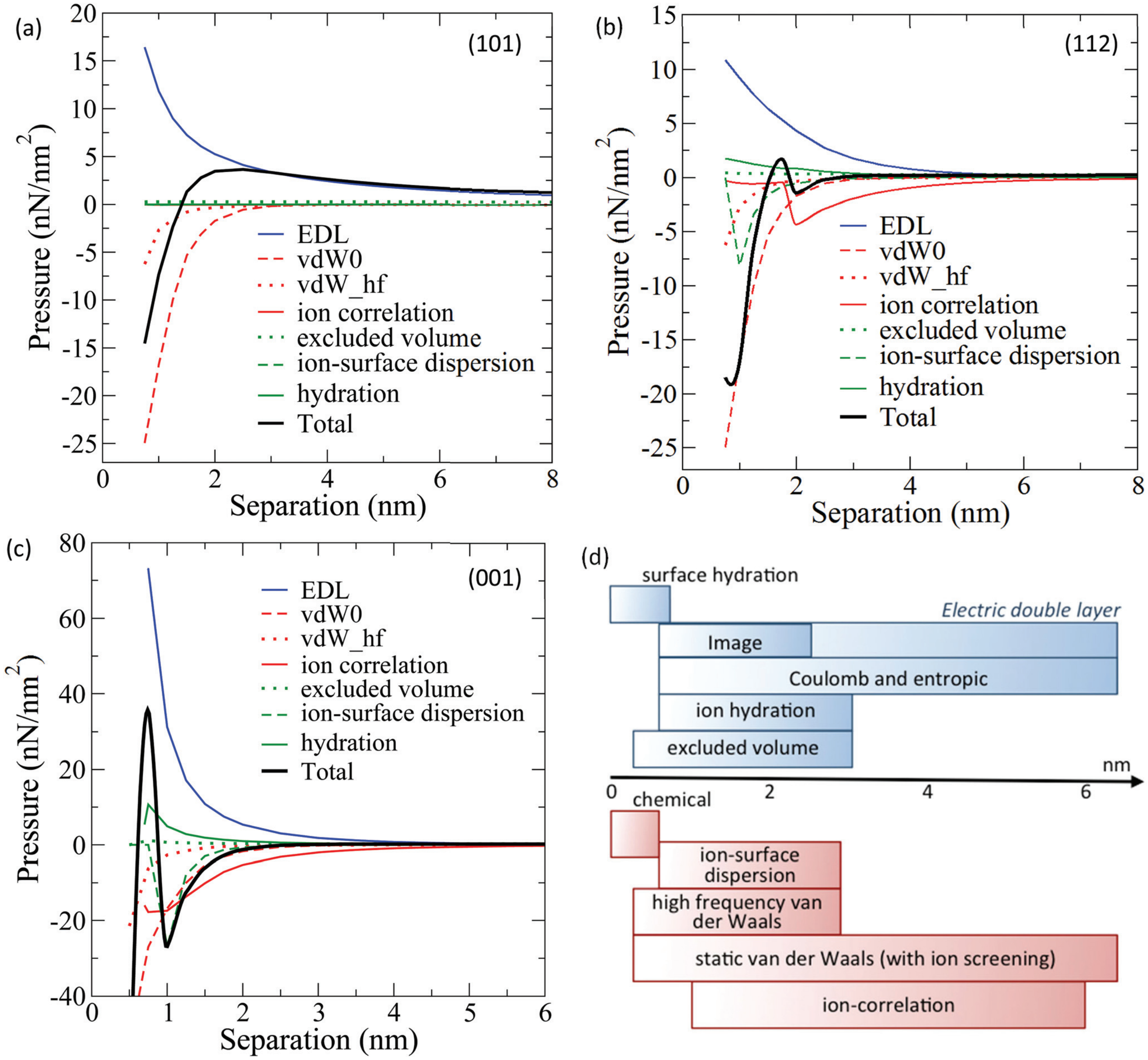

Fig. 3 Distance dependence of the components of the total disjoining pressure between two anatase (101) facets (a), two (112) facets (b) and two (001) facets (c) at pH 3, and (d) a general schematic of attractive (red) and repulsive (blue) forces and their ranges. The EDL pressure includes direct Coulomb and image contributions, vdW0 and vdW_hf stand for zero frequency (static) and high frequency van der Waals interactions between nanoparticles, respectively. The hydration term stands for hydration pressure arising from ion–water interactions.

(3) *Adhesion*: On physical contact between the aligned or nearly aligned lattices, or equivalently in the vicinity of the primary minimum of the particle–particle interaction force curve, the adhesion process occurs driven by forces that have a chemical nature, *e.g.*, chemical bonding and interatomic van der Waals forces. These forces drive the rotation of nearly aligned lattices to perfect alignment, the exclusion of any remaining solvent, elimination of defects and the fusing of the two lattices.[3] An example of these interactions was shown through molecular simulations for anatase nanoparticles, which demonstrated that the face dependence of adhesion is linked to different levels of hydrophilicity for different crystal terminations.[20,21]

Ion correlation and ion-surface dispersion forces are non-mean field attractive contributions giving rise to face specific interactions in a relatively long range. Ion correlation forces, which arise from coupled fluctuations in ionic densities in the diffuse layer, a second order electrostatic interaction, are sensitive to the details of the distribution of charged groups on the nanoparticle surfaces, which, in turn, depend on the crystallographic face. These interactions are the mesoscopic analogues to the microscopic interactions between fluctuating induced dipoles, or atom–atom van der Waals forces. On the nanometer scale the fluctuating electric field is created by the fluctuations in ion densities in the interacting diffuse layers of two solvent-separated surfaces. In many cases these interactions lead to the overall attractive interactions between like-charged surfaces[44] or polyelectrolytes even under low salt conditions.[45]

Our simulations revealed a complex dependence of these ion correlation forces on interparticle separation. Attractive ion correlation pressure monotonically increases reaching a maximum at 2 nm separation for the (112) faces and 0.8 nm for the (001) faces (Fig. 3). Although for the (112) faces the maximum ion correlation attraction is smaller than for the (001) faces, these attractive interactions are of longer range. The onset of attraction due to ion correlation forces is at 6 nm separation for the (112) faces, while for the (001) faces these interactions only become significant below 4 nm, with total particle–particle interactions becoming attractive at 3 nm and 2.5 nm separations, respectively. For the (112) surfaces the ion correlation pressure decreases markedly at 1.75 nm separation (Fig. 3b). Such an effect could conceivably be due to "ion pinning" in the EDL by the close packed hexagonal array of surface charges on the (112) faces, resulting in a significant decrease in fluctuations in ionic density in the EDL. This effect gives rise to a shallow barrier between the primary and secondary minima on the pressure curve for the (112) faces and is not observed for the (001) faces with a square lattice of surface charges.

At an even closer approach, below 0.75 nm separation, the pressure curve is marked by a rapid decrease in ion-induced attractive interactions (Fig. 3). Ion-surface dispersion and ion correlation forces start decreasing for all faces as ions start leaving the gap between the nanoparticles. At these separations, ions and surfaces start competing for hydration water and it becomes more energetically favorable for the non-adsorbed ions to be expelled from the gap between nanoparticles into bulk solution, where they retain their hydration shell. In our simulations there are no free ions left in the gap at separations of 0.5 nm, a finding consistent with MD simulations.[46] Experimental observations indirectly point to the expulsion of ions from the gap between the surfaces at separations of 0.4 nm, manifested in the onset of exponential repulsive surface–surface hydration interactions, independent of the ionic concentration or the nature of the electrolyte.[42]

Several opposing factors underlie the overall pH dependence of ion correlation forces in the capture minimum region of the pressure–distance curve. At 2 nm separation between the nanoparticles the EDLs are separated by a layer of "bulk solution". In this regime the strength of ion correlation forces is defined by the thickness of the EDL, the effective 2D ion density in the EDL, which increases with ion concentration or surface charge density, and the effective distance between the EDLs. The EDL thickness, characterized by the Debye length, decreases with the increasing electrolyte concentration. In contrast, the effective distance between the EDLs at fixed separation between the interacting surfaces and the 2D ion density in the EDL increases with the increasing electrolyte concentration. Overall, the combination of these opposing effects results in a non-monotonic dependence of ion-correlation forces on the electrolyte concentration or pH (Fig. 2).

We note that early theories of ion correlation forces in electrolytes confined between two uniformly charged plates or cylinders predict the insignificant contribution of ion correlations in monovalent electrolytes and conclude that in order to induce attraction between two like-charged surfaces the counterion valency should be two and above. However, experimental evidence points to attractive interactions between like-charged polyelectrolytes in low concentration monovalent electrolyte solutions,[45] suggesting that these early theories are missing some important detail. As we show here and in our recent work on ionic atmospheres around DNA[33] taking the approximation of a uniformly charged surface (*i.e.*, a continuum distribution as opposed to a structurally based distribution of charge) cannot be used when treating ion correlations. Introducing a discrete distribution of charged groups and the topography of surfaces/polyelectrolytes into the treatment of ion correlations gives rise to strong attractive ion correlation forces between surfaces (Fig. 3) and to a highly structured ionic atmosphere of monovalent counterions around DNA, in good agreement with molecular dynamics simulations, but in contrast with Poisson–Boltzmann simulations (no ion correlations) within the same model of DNA.[33] The simulation results of the present study further reinforce the notion that the origin of the ion correlation attractive force lies in a discretized distribution of charge across an interface, based in this case on the distinct oxygen sublattice structures of the different facets of anatase.

Ion correlation forces not only play a central role in face selectivity during the nanoparticle approach, but also are strong enough in the long-range to influence the mutual orientation of the interacting nanoparticles in the vicinity of the capture minimum. Our simulations reveal a clear angular dependence of ion-correlation interactions between two (112) anatase faces with a half-period of 30°, as expected from the hexagonal symmetry of the surface charge distribution on this face (Fig. 4). Moreover, the strongest attractive force is observed for 15° angular displacement between the two oxygen lattices, corresponding to a low-index oxygen plane that can be found in the adjacent layers of a continuous anatase crystal. The second energetically favorable orientation was found to be the configuration in which one oxygen sublattice is translationally shifted by half of a surface unit cell spacing and rotated by 15° with respect to the other lattice (Fig. 4). This latter configuration corresponds to an oxygen sublattice arrangement at a {112} contact twin boundary. These results agree with the experimental observation of the formation of either a perfect defect free crystal or a twin boundary in the OA process.[14]

Summarizing the results for TiO_2, our simulations predict that facet specific attractive interactions between nanoparticles dominate the interactions in the solvent separated state in a very narrow pH range from pH 2.5 to 3.5, in agreement with the experimental observation that OA between anatase crystals is most probable at pH 3, while random aggregation is more

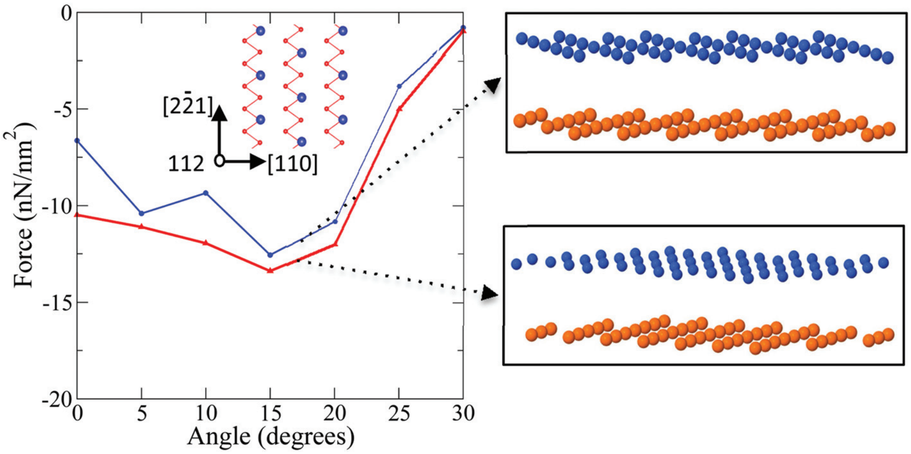

Fig. 4 Angular dependence of the ion-correlation forces at the midplane between (112) anatase facets at 3 nm interparticle separation and the corresponding arrangement of surface oxygens on the interacting facets. Angle is defined as the angle for the in-plane rotation of one surface with respect to the other around the rotation axis perpendicular to the interacting facets. Angular dependencies were calculated starting from the identical configuration of oxygen sublattices on the interacting surfaces at 0° (triangles, red line) and starting from the configuration with the top oxygen lattice shifted by half of a unit cell in [221] and [110] directions (circles, blue line). Protonated oxygens on the surface of one nanoparticle are shown in orange and on the other in blue. The inset shows oxygen sublattice on anatase (112) surface (red spheres) and the corresponding lattice of protonated oxygens (blue spheres) at pH 3.

probable at pH 1.2–2.1 and pH 8–11.[14] Furthermore, at pH 3 simulations predict that, driven by ion-correlation forces, the OA takes place along the (112) anatase faces leading to the formation of either a perfect crystal or a twin boundary, also in agreement with experimental observations.[14]

To further demonstrate the role of mesoscale forces in nanoparticle alignment preceding OA and the transferability of the model to other systems we considered ZnO nanoparticles in methanol solutions of zinc acetate dihydrate. The details of crystal growth in these solutions were studied experimentally by Weller *et al.*[47] To summarize the experimental findings, the growth of spherical nanoparticles was observed in 0.01 M zinc acetate dihydrate solutions at room and elevated temperatures, and no nanoparticle aggregation or oriented attachment was observed. A 10× increase in electrolyte concentration and heating was found to be an essential prerequisite for ZnO nanorod growth.[47] The resulting ZnO nanorods had a wurtzite structure and grew along the *c*-direction *via* oriented attachment of nanoparticles along ZnO (0001) faces.[47]

Nanorod growth along the *c*-direction requires the presence of attractive interactions between O- and Zn-terminated ZnO (0001) faces. These surfaces are polar and due to a significant surface dipole the pristine stoichiometric (0001) surfaces are not stable without reconstruction and/or hydroxylation in the presence of water.[48,49] Although the details of surface chemistry of these ZnO faces are still debated in the literature, experimental and theoretical findings point to surface stabilization *via* the formation of charged vacancies and pits in a vacuum[48–50] and to partial hydroxylation in the presence of water.[51–55] The experiments by Weller *et al.*[47] were performed in the presence of water and under alkaline conditions, which favors partial hydroxylation of ZnO (0001) faces. Given that the pristine (0001) faces of ZnO have a hexagonal lattice of oxygens (or Zn for Zn-terminated surface) the arrangement of charged defects (adsorbates) on the Zn (0001) faces is similar to that on the anatase TiO_2 {112} faces. As demonstrated for anatase, the close packed hexagonal distribution of charged defects on the interacting crystal faces leads to the maximum attractive ion correlation interactions for a given surface charge density, *e.g.* for a given pH and electrolyte concentration. Qualitatively this explains the OA along the (0001) faces and ZnO nanorod growth in the *c*-direction.

To connect with experimental observations on a more quantitative level we considered the effect of the electrolyte concentration and temperature on the interactions between the ZnO (0001) faces. In particular, we considered the interactions between the O-terminated and Zn-terminated ZnO (0001) faces, which have to come into direct contact for nanorod formation. Based on experimental observations for the concentration of charged defects on ZnO (0001) faces,[52] 25% of surface oxygens were protonated on the O-terminated surface and 25% of Zn were hydroxylated on the Zn-terminated surface, respectively. Simulations revealed that the interactions between these oppositely charged surfaces follow the mean-field behavior for separations above 7 nm and are weakly attractive (data not shown). This attraction is followed by a repulsive barrier at a closer approach, followed by attraction at 0.5 nm separation (Fig. 5a). Although the pressure–distance curves are qualitatively similar in 0.01 M and 0.1 M solutions at room temperature and at 55 °C, the quantitative differences are profound (Fig. 5a). In 0.01 M solution at 25 °C the long range attractive interactions are very weak with a maximum attractive pressure as low as -2×10^{-6} nN nm^{-2}, while the repulsive barrier is as high as 4.6×10^{-2} nN nm^{-2}. This barrier is almost 7 times higher than the short range attractive inter-

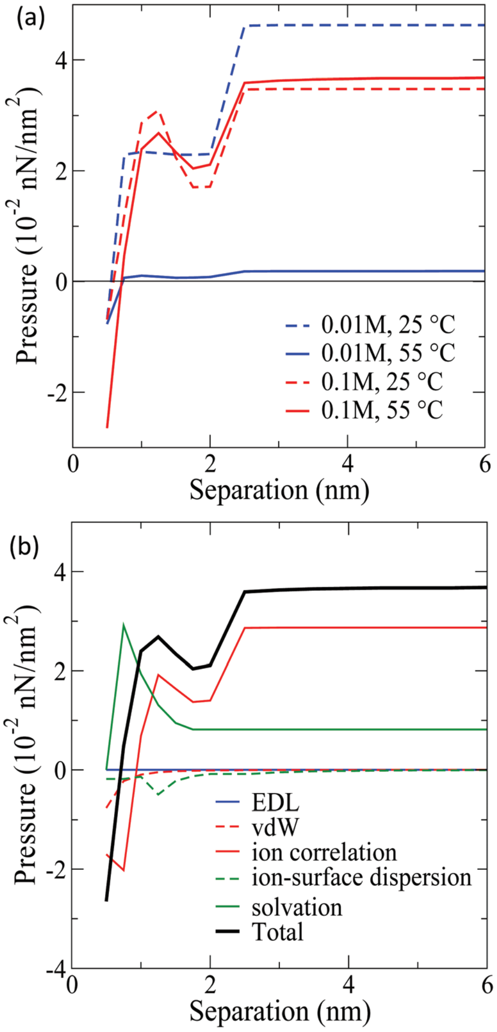

Fig. 5 Distance dependence of the disjoining pressure between the Zn-terminated and O-terminated ZnO (0001) facets in a methanol solution of zinc acetate dihydrate. (a) Total disjoining pressure in solutions with *c* concentration 0.01 M (blue lines) and 0.1 M (red lines) at 25 °C (dashed lines) and 55 °C (solid lines). (b) Components of the disjoining pressure in solutions with 0.1 M zinc acetate dihydrate at 55 °C. The EDL pressure includes direct Coulomb and image contributions and it is close to zero for all separations studied, vdW indicates van der Waals interactions between nanoparticles. The solvation term stands for solvation pressure arising from ion–methanol interactions.

actions at 0.5 nm separation and the interactions between the ZnO (0001) faces at room temperature can be considered purely repulsive, which is in line with the experimental observation that ZnO nanoparticles do not aggregate under these conditions and grow *via* classical ion addition.[47] The interactions between the nanoparticles in the same solution, but at elevated temperatures, are weak over the whole range of interparticle distance studied (Fig. 5a) and these particles can be considered non-interacting, also suggesting the absence of aggregation or attachment. The increase in salt concentration to 0.1 M leads to the lowering of the repulsive barrier at room temperature to 3.5×10^{-2} nN nm^{-2} and to the appearance of a local minimum in the repulsive region at 2 nm separation. Nonetheless, the long-range attractive interactions are the same as in 0.01 M solution and the attraction at 0.5 nm is 5 times smaller than the repulsive barrier, making the aggregation or attachment energetically unfavorable, also in-line with experimental observations. Only at 55 °C does the attachment between the O-terminated and Zn-terminated (0001) faces becomes possible. At this elevated temperature and salt concentration the long range attractive interactions become 3 orders of magnitude larger than that in all previous cases and equal to 7.5×10^{-3} nN nm^{-2} (data not shown). Such relatively strong long-range attraction should facilitate particle capture in the orientation required for nanowire growth. Given that there is still a significant barrier at 3–7 nm separations, it is likely that the subsequent growth process will involve growth of the trapped particles *via* classical ion addition before jump to contact and attachments take place. Three features of the pressure curves facilitate the oriented attachment of trapped nanoparticles under these conditions: (i) the short-range attraction is comparable to the repulsive barrier height; (ii) the minimum in the repulsive region is shallow and (iii) the barrier height separating this shallow minimum and the attractive minimum is low. The combination of these effects supports the oriented attachment of ZnO nanoparticles along the O-terminated and Zn-terminated (0001) faces in 0.1 M electrolyte at 55 °C.

The analysis of the contributions to the disjoining pressure for this solvent composition and temperature revealed a non-mean field character of the interactions up to separations of 6.5 nm (Fig. 5b). Only beyond this distance range do the non-mean field contributions compensate each other and DLVO-type behavior is recovered. Similar to anatase TiO_2 in aqueous electrolyte solutions, for ZnO in methanol electrolyte, ion-correlation forces and ion solvation interactions dominate interparticle interactions at 0.5–6.5 nm separations (Fig. 5b). It is remarkable that the dominating interactions are responsible for particle mutual orientation and have the same fundamental nature in such different systems. Namely, for anatase particles, alignment and capture take place along like-charged faces in a low concentration electrolyte in aqueous solution at room temperature, while for ZnO the alignment occurs along oppositely charged faces in a high concentration electrolyte in methanol and at elevated temperatures. The common prerequisite for facet selectivity and particle alignment that emerges from this study is the requirement of a close packed arrangement of charged species on the interacting surfaces. For oxides in water-containing solutions such charged species are usually acquired through partial protonation/hydroxylation of the surfaces. Then the distribution of discrete charges on the surface is dictated by surface atomic ordering and by the pH and electrolyte concentration. Alternatively, a desired distribution of charged species on specific crystal faces can be engineered through targeted surface functionalization with ligands. This approach, which is often used successfully in material synthesis, includes assembly of ordered nanostructures *via* oriented attachment of functionalized nanocrystals.[6,12,56] Once the desired surface chemistry is achieved, the interparticle forces can be further tuned by adjusting the properties of the electrolyte including the nature of ions, their size, charge and solvation properties. All these system variables affect the strength of the dominating forces, ion-correlation and solvation, and can be finely adjusted through the choice of electrolyte. As demonstrated using the example of ZnO, temperature is also an important factor defining the strength of entropic ion-correlation forces between the nanoparticles, and is instrumental in shifting the balance of interactions from enthalpic solvation repulsion to entropic ion-correlation attraction.

We note that ZnO nanorod growth takes place at elevated temperatures and non-equilibrium effects, such as spontaneous dipolar polarization,[57] may contribute to directing the OA. As discussed above, the ideal ZnO (0001) surfaces are polar and the corresponding ideal ZnO (0001)-terminated nanorods would have a considerable macroscopic dipole. Under equilibrium conditions these macroscopic dipoles are compensated *via* the formation of surface defects and partial hydroxylation/protonation of the (0001) faces. Under non-equilibrium conditions, however, a total compensation of the macroscopic dipole may not be achieved. Then the residual dipolar polarization would also contribute to interparticle interactions. In contrast, experiments on anatase TiO_2 OA were performed over a long period of time at room temperature and anatase facets can be considered to be in equilibrium with solution. Therefore, spontaneous polarization is not likely to be significant or orientation specific.

Discussion

Our study revealed the dual role of metal oxide surface chemistry in controlling the oriented attachment process in electrolyte solutions. On one hand, surface chemistry defines the strength of short-range adhesion forces and their facet specificity, as demonstrated in ref. 21 for anatase TiO_2. On the other hand, the current study revealed that surface chemistry also has a profound effect on the structure and fluctuation dynamics in electrolyte solutions giving rise to face specific mesoscale interactions. These solvent mediated interactions acting on the approaching nanoparticles at separations higher than 0.5 nm propagate the information on surface chemistry well beyond the range of chemical forces. This phenomenon is crucial in the oriented attachment process. It allows nanoparticles to explore the complex free energy landscape while in the solvent separated state before jump to contact takes place and short-range chemical forces take over the adhesion process.[3,11,12] These mesoscale solvent mediated interactions, or ion correlation forces, are sensitive to the details of the distribution of discrete charged species on the interacting surface. For metal oxides in the presence of water these charged species often arise from partial hydroxylation or protonation of nanoparticle surfaces, which is one of the most fundamental surface stabilization mechanisms for these materials. The strength of ion correlation forces can be finely tuned by varying the concentration, charge, size and polarisability of electrolyte ions, the solvent dielectric constant, and the temperature providing a versatile mechanism for controlling particle based crystal growth and materials synthesis. On the down side, such sensitivity of ion correlation forces to multiple parameters of the electrolyte solutions and to nanoparticle surface chemistry requires computational approaches that go beyond a mean-field approximation. The classical DFT model presented here provides one such method.

In this work we focused on elucidating the role of surface chemistry in face and orientation specific long- and short-range interparticle interactions. For metal oxides in aqueous electrolyte solutions surface chemistry is mainly defined by the interaction of the mineral surface with water and can be controlled by tuning the electrolyte properties. Alternatively, surface chemistry can be purposely modified by ligands to facilitate and direct the OA process.[58–60] Ligands can play several roles including capping agents, which prevent aggregation along specific crystal faces thereby directing the OA along the faces not protected by ligands. Charged ligands can be used to engineer the surface charge density of the interacting nanoparticles, which, in turn, modifies solvent-mediated interparticle forces, shifting the balance of interactions from that favoring random aggregation to OA along specific crystal faces.[58–60] For small ligands, which can be approximated as a single coarse-grained unit, as was done, for example, in a recent study of ligand mediated cation exchange in PbS nanocrystals,[61] the presented model can be readily applied with face specific ligand-surface short-range interactions derived from plane-wave DFT (see the ESI†). Ligands are then considered as extra mobile species along with ions and solvent molecules. To adapt the presented framework to modeling more complex OA processes directed by polymeric ligands the classical DFT formalism needs to include an additional term describing chain connectivity within the ligands. One of the common methods for calculating the correlation free energy due to chain connectivity is based on thermodynamic perturbation theory, which was successfully used for predicting surfactant and polymer assembly in solution and at surfaces.[62–67] With this extension to the current model, the presented computational framework can be used for describing the role of the reaction temperature, concentration of the reactants, and the concentration and chemistry of stabilizing agents, the key variables in the one-step synthesis of nanostructures *via* OA,[56] to direct the OA-based synthesis of nanostructures. We note that for some materials, apart from solvent mediated micro- and mesoscopic interactions discussed here, macroscopic forces arising from dielectric,[68–70] electric[57,71] and magnetic anisotropy also need to be considered for a comprehensive picture of orientation dependent interactions.[72] For example, rutile TiO_2 is strongly dielectrically anisotropic[73] and orientation specific macroscopic van der Waals interactions are expected to play an important role in particle alignment. Even in dielectrically isotropic materials macroscopic van der Waals interactions may exhibit significant anisotropy due to the shape dependence of these interactions.[74] In particular, recent studies showed that shape-anisotropic van der Waals interactions play an important role in the growth of 1D and 2D structures *via* OA.[75–79] Other examples of OA driven by macroscopic interactions include particle-based growth of CdTe nanowires, which is thought to be driven by macroscopic dipole–dipole interparticle interactions.[80] We note that although ligands were used in that work as surface stabilizing agents for CdTe nanoparticles they were not considered to contribute to facet selectivity and alignment and their controlled removal was a necessary step for oriented attachment.[80] Finally, external fields including mechanical stress, electric and magnetic fields can direct oriented attachment of nanoparticles.[81] Quantifying the effects of macroscopic orientation dependent forces in the oriented attachment process falls beyond the scope of the current study, which focuses on materials with isotropic bulk electromagnetic properties, and our findings on the effect of anisotropic macroscopic forces on the orientation dependence of interparticle interactions will be reported elsewhere.

Methods

Simulations were performed using full molecular representation of electrolyte solutions. Ions are modeled as spheres with Pauling ionic diameters and water as spheres with van der Waals diameter and an experimental density of 55.5 M. Nanoparticles are modeled as rectangular slabs with discrete charge distribution on the interacting facets. The position of charges corresponds to the atomic position of charged groups on the oxygen sublattice of anatase surfaces. The simulation cell is 10 nm × 30 nm × 10 nm in size with nanoparticle faces of 3 nm × 3 nm. Interactions between all the species are treated within classical density functional theory (classical DFT) and include short-range pair-wise solvation interactions, many-body interactions arising from ion and water electrodynamic, electrostatic (up to second order) and excluded volume interactions, and van der Waals particle–particle interactions (see the ESI† for details). In the spirit of the density functional theory all components of the free energy, except particle–particle van der Waals interactions, are formulated in terms of the densities of mobile species, ions and water. Such reformulation of the many-body free energy, which depends on coordinates of all atoms in the simulation cell ($3N$ spatial variables, where N is the number of atoms), in terms of the densities of each atom type reduces the number of spatial variables to 3 × (number of atom types) while retaining atomistic spatial resolution and provides the required computational efficiency. Static free energy minimization simulations were performed in three-dimensions with subatomic resolution of ionic and water densities and chemical potentials using the numerical procedure described in ref. 82. The model was tested against the experimental data for ion activity in the 0–2 M range and ion counting anomalous small angle X-ray scattering experiments for the ionic atmosphere around DNA.[33]

Conclusions

In summary, atomistic simulations were developed that reach for the first time into the mesoscale for OA, to reveal the origin of face specificity for forces that attract and orient anatase TiO_2 nanoparticles in aqueous electrolyte solutions within a solvent-separated state. These simulations are complementary to previously reported reactive molecular dynamics data in the adhesion regime[20,21] and provide new insights into the nature and balance of attractive and repulsive forces acting on nanoparticles in the capture minimum regime, which turn out to be dominated by ion correlation forces. The dispersion interactions of diffuse layer counterions from the opposing interfaces yield a net attractive force that creates a stable minimum on the pressure–distance curve. The presence of this minimum allows captured nanoparticles to explore the energy landscape with respect to their mutual orientation while in the solvent-separated state, ultimately enabling successful adhesion events and OA. Our model demonstrates that the forces operating in the capture minimum regime are sufficient to cause particles to optimize their mutual orientation into co-alignment while separated by layers of the solvent. We show that this fine adjustment of mutual orientation of the interacting faces is also driven by ion correlation forces, leading to the formation of either a perfect crystal or a twin boundary, in agreement with experimental observations. These results provide a direct link between the solution composition and the pathway for particle-based crystallization essential for knowledge-based design of highly ordered nanostructured materials.

Acknowledgements

This study is based upon work supported by the U.S. Department of Energy (DOE) Office of Science, Office of Basic Energy Sciences, Chemical Sciences, Geosciences, and Biosciences Division, through its Geosciences Program at Pacific Northwest National Laboratory (PNNL). The modeling approach was developed through support of the Materials Synthesis and Simulations across Scales (MS^3) Initiative, a Laboratory Directed Research and Development Program at PNNL. PNNL is a multiprogram national laboratory operated by Battelle for the DOE. Simulations were performed using PNNL Institutional Computing resources. We thank Jim De Yoreo for fruitful discussions.

Notes and references

1 N. Gehrke, H. Colfen, N. Pinna, M. Antonietti and N. Nassif, *Cryst. Growth Des.*, 2005, **5**, 1317–1319.
2 V. K. Ivanov, P. P. Fedorov, A. Y. Baranchikov and V. V. Osiko, *Russ. Chem. Rev.*, 2014, **83**, 1204–1222.
3 D. S. Li, M. H. Nielsen, J. R. I. Lee, C. Frandsen, J. F. Banfield and J. J. De Yoreo, *Science*, 2012, **336**, 1014–1018.

4 R. L. Penn and J. F. Banfield, *Am. Mineral.*, 1998, **83**, 1077–1082.

5 R. L. Penn and J. F. Banfield, *Science*, 1998, **281**, 969–971.

6 M. P. Boneschanscher, W. H. Evers, J. J. Geuchies, T. Altantzis, B. Goris, F. T. Rabouw, S. A. P. van Rossum, H. S. J. van der Zant, L. D. A. Siebbeles, G. Van Tendeloo, I. Swart, J. Hilhorst, A. V. Petukhov, S. Bals and D. Vanmaekelbergh, *Science*, 2014, **344**, 1377–1380.

7 H. Colfen and M. Antonietti, *Angew. Chem., Int. Ed.*, 2005, **44**, 5576–5591.

8 A. Navrotsky, *Proc. Natl. Acad. Sci. U. S. A.*, 2004, **101**, 12096–12101.

9 R. Q. Song and H. Colfen, *Adv. Mater.*, 2010, **22**, 1301–1330.

10 V. M. Yuwono, N. D. Burrows, J. A. Soltis and R. L. Penn, *J. Am. Chem. Soc.*, 2010, **132**, 2163–2165.

11 M. H. Nielsen, D. S. Li, H. Z. Zhang, S. Aloni, T. Y. J. Han, C. Frandsen, J. Seto, J. F. Banfield, H. Colfen and J. J. De Yoreo, *Microsc. Microanal.*, 2014, **20**, 425–436.

12 J. J. De Yoreo, P. U. P. A. Gilbert, N. A. J. M. Sommerdijk, R. L. Penn, S. Whitelam, D. Joester, H. Z. Zhang, J. D. Rimer, A. Navrotsky, J. F. Banfield, A. F. Wallace, F. M. Michel, F. C. Meldrum, H. Colfen and P. M. Dove, *Science*, 2015, **349**, 6760.

13 N. D. Burrows, C. R. H. Hale and R. L. Penn, *Cryst. Growth Des.*, 2013, **13**, 3396–3403.

14 R. L. Penn and J. F. Banfield, *Geochim. Cosmochim. Acta*, 1999, **63**, 1549–1557.

15 N. Alcantar, J. Israelachvili and J. Boles, *Geochim. Cosmochim. Acta*, 2003, **67**, 1289–1304.

16 Q. Y. Tan, G. T. Zhao, Y. H. Qiu, Y. J. Kan, Z. H. Ni and Y. F. Chen, *Langmuir*, 2014, **30**, 10845–10854.

17 F. Huang, B. Gilbert, H. H. Zhang and J. F. Banfield, *Phys. Rev. Lett.*, 2004, **92**, 155501.

18 H. Z. Zhang and J. F. Banfield, *J. Phys. Chem. Lett.*, 2012, **3**, 2882–2886.

19 D. S. Li, F. Soberanis, J. Fu, W. T. Hou, J. Z. Wu and D. Kisailus, *Cryst. Growth Des.*, 2013, **13**, 422–428.

20 K. A. Fichthorn, *Chem. Eng. Sci.*, 2015, **121**, 10–15.

21 M. Raju, A. C. T. van Duin and K. A. Fichthorn, *Nano Lett.*, 2014, **14**, 1836–1842.

22 H. Z. Zhang, J. J. De Yoreo and J. F. Banfield, *ACS Nano*, 2014, **8**, 6526–6530.

23 B. Derjaguin and L. Landau, *Zh. Eksp. Teor. Fiz.*, 1945, **15**, 663–682.

24 E. J. W. Verwey, *Philips Res. Rep.*, 1945, **1**, 33–49.

25 E. J. W. Verwey, *J. Phys. Colloid Chem.*, 1947, **51**, 631–636.

26 N. D. Burrows, C. R. H. Hale and R. L. Penn, *Cryst. Growth Des.*, 2012, **12**, 4787–4797.

27 J. Israelachvili, *Intermolecular and Surface Forces*, Academic Press, New York, 1991.

28 *CRC handbook of chemistry and physics*, CRC Press, London, England, 2014.

29 D. J. Tobias, A. C. Stern, M. D. Baer, Y. Levin and C. J. Mundy, *Annu. Rev. Phys. Chem.*, 2013, **64**, 339–359.

30 L. Tuma, D. Jenicek and P. Jungwirth, *Chem. Phys. Lett.*, 2005, **411**, 70–74.

31 B. Medasani, Z. Ovanesyan, D. G. Thomas, M. L. Sushko and M. Marucho, *J. Chem. Phys.*, 2014, **140**, 204510.

32 Y. C. Liu, Q. Wang and L. H. Lu, *Chem. Phys. Lett.*, 2003, **381**, 210–215.

33 M. L. Sushko, D. G. Thomas, S. A. Pabit, L. Pollack, A. V. Onufriev and N. A. Baker, *Biophys. J.*, 2016, **110**, 315–326.

34 M. L. Sushko and K. M. Rosso, *MRS Online Proc. Libr.*, 2015, 1753, DOI: 10.1557/opl.2015.1108.

35 M. Mikami, S. Nakamura, O. Kitao and H. Arakawa, *Phys. Rev. B: Condens. Matter*, 2002, **66**, 155213.

36 G. A. Parks, *Rev. Mineral.*, 1990, **23**, 133–175.

37 M. P. Finnegan, H. Z. Zhang and J. F. Banfield, *Chem. Mater.*, 2008, **20**, 3443–3449.

38 J. P. Holmberg, E. Ahlberg, J. Bergenholtz, M. Hassellov and Z. Abbas, *J. Colloid Interface Sci.*, 2013, **407**, 168–176.

39 J. R. Rustad, A. R. Felmy and B. P. Hay, *Geochim. Cosmochim. Acta*, 1996, **60**, 1553–1562.

40 R. L. Penn and J. A. Soltis, *CrystEngComm*, 2014, **16**, 1409–1418.

41 X. G. Xue, R. L. Penn, E. R. Leite, F. Huang and Z. Lin, *CrystEngComm*, 2014, **16**, 1419–1429.

42 S. Leikin, V. A. Parsegian, D. C. Rau and R. P. Rand, *Annu. Rev. Phys. Chem.*, 1993, **44**, 369–395.

43 E. Schneck, F. Sedlmeier and R. R. Netz, *Proc. Natl. Acad. Sci. U. S. A.*, 2012, **109**, 14405–14409.

44 P. A. Pincus and S. A. Safran, *Europhys. Lett.*, 1998, **42**, 103–108.

45 G. S. Manning, *Eur. Phys. J. E*, 2011, **34**, 132.

46 Y. S. Leng, *Langmuir*, 2012, **28**, 5339–5349.

47 C. Pacholski, A. Kornowski and H. Weller, *Angew. Chem., Int. Ed.*, 2002, **41**, 1188–1191.

48 R. Wahl, J. V. Lauritsen, F. Besenbacher and G. Kresse, *Phys. Rev. B: Condens. Matter*, 2013, **87**, 085313.

49 G. Kresse, O. Dulub and U. Diebold, *Phys. Rev. B: Condens. Matter*, 2003, **68**, 245409.

50 H. Xu, L. Dong, X. Q. Shi, M. A. Van Hove, W. K. Ho, N. Lin, H. S. Wu and S. Y. Tong, *Phys. Rev. B: Condens. Matter*, 2014, **89**, 235403.

51 H. G. Ye, G. D. Chen, H. B. Niu, Y. Z. Zhu, L. Shao and Z. J. Qiao, *J. Phys. Chem. C*, 2013, **117**, 15976–15983.

52 A. Onsten, D. Stoltz, P. Palmgren, S. Yu, M. Gothelid and U. O. Karlsson, *J. Phys. Chem. C*, 2010, **114**, 11157–11161.

53 M. Schiek, K. Al-Shamery, M. Kunat, F. Traeger and C. Woll, *Phys. Chem. Chem. Phys.*, 2006, **8**, 1505–1512.

54 J. B. L. Martins, V. Moliner, J. Andres, E. Longo and C. A. Taft, *J. Mol. Struct. (THEOCHEM)*, 1995, **330**, 347–351.

55 J. A. Rodriguez and C. T. Campbell, *Surf. Sci.*, 1988, **197**, 567–593.

56 K. S. Cho, D. V. Talapin, W. Gaschler and C. B. Murray, *J. Am. Chem. Soc.*, 2005, **127**, 7140–7147.

57 B. L. Fan, Y. M. Zhang, R. L. Yan and J. Y. Fan, *CrystEngComm*, 2016, **18**, 6492–6501.

58 C. G. Lu and Z. Y. Tang, *Adv. Mater.*, 2016, **28**, 1096–1108.

59 J. J. Geuchies, C. van Overbeek, W. H. Evers, B. Goris, A. de Backer, A. F. Gantapara, F. T. Rabouw, J. Hilhorst,

J. L. Peters, O. Konovalov, A. V. Petukhov, M. Dijkstra, L. D. A. Siebbeles, S. van Aert, S. Bals and D. Vanmaekelbergh, *Nat. Mater.*, 2016, DOI: 10.1038/nmat4746.

60 J. Novak, R. Banerjee, A. Kornowski, M. Jankowski, A. Andre, H. Weller, F. Schreiber and M. Scheele, *ACS Appl. Mater. Interfaces*, 2016, **8**, 22526–22533.

61 Z. C. Fan, L. C. Lin, W. Buijs, T. J. H. Vlugt and M. A. van Huis, *Nat. Commun.*, 2016, **7**, 11503.

62 S. Jain, A. Dominik and W. G. Chapman, *J. Chem. Phys.*, 2007, **127**, 244904.

63 S. Tripathi and W. G. Chapman, *Phys. Rev. Lett.*, 2005, **94**, 087801.

64 J. P. Donley, J. J. Rajasekaran, J. D. Mccoy and J. G. Curro, *J. Chem. Phys.*, 1995, **103**, 5061–5069.

65 J. Z. Wu and Z. D. Li, *Annu. Rev. Phys. Chem.*, 2007, **58**, 85–112.

66 M. L. Sushko and J. Liu, *J. Phys. Chem. B*, 2011, **115**, 4322–4328.

67 D. P. Cao and J. Z. Wu, *J. Chem. Phys.*, 2005, **122**, 194703.

68 V. A. Parsegian and R. Podgornik, *Biophys. J.*, 2004, **86**, 38A–38A.

69 P. Va and G. H. Weiss, *J. Adhes.*, 1972, **3**, 259.

70 D. M. Dryden, J. C. Hopkins, L. K. Denoyer, L. Poudel, N. F. Steinmetz, W. Y. Ching, R. Podgornik, A. Parsegian and R. H. French, *Langmuir*, 2015, **31**, 10145–10153.

71 W. D. He, *CrystEngComm*, 2014, **16**, 1439–1442.

72 W. Q. Lv, W. D. He, X. N. Wang, Y. H. Niu, H. Q. Cao, J. H. Dickerson and Z. G. Wang, *Nanoscale*, 2014, **6**, 2531–2547.

73 S. Schoche, T. Hofmann, R. Korlacki, T. E. Tiwald and M. Schubert, *J. Appl. Phys.*, 2013, **113**, 164102.

74 J. C. Hopkins, R. Podgornik, W. Y. Ching, R. H. French and V. A. Parsegian, *J. Phys. Chem. C*, 2015, **119**, 19083–19094.

75 A. E. Marzbanrad, G. Rivers, A. Rogalsky, P. Lee-Sullivan, B. X. Zhao and N. Y. Zhou, *RSC Adv.*, 2016, **6**, 61641–61649.

76 A. L. Chen, Y. Zhou, S. Miao, Y. Li and W. J. Shen, *CrystEngComm*, 2016, **18**, 580–587.

77 K. C. Wen and W. D. He, *Nanotechnology*, 2015, **26**, 382001.

78 W. Q. Lv, W. R. Huo, Y. H. Niu, Y. X. Zhu, Y. T. Xie, X. Y. Guo and W. D. He, *CrystEngComm*, 2015, **17**, 729–733.

79 W. Q. Lv, X. M. Yang, W. Wang, Y. H. Niu, Z. P. Liu and W. D. He, *ChemPhysChem*, 2014, **15**, 2688–2691.

80 Z. Y. Tang, N. A. Kotov and M. Giersig, *Science*, 2002, **297**, 237–240.

81 Z. W. Wang, C. Schliehe, T. Wang, Y. Nagaoka, Y. C. Cao, W. A. Bassett, H. M. Wu, H. Y. Fan and H. Weller, *J. Am. Chem. Soc.*, 2011, **133**, 14484–14487.

82 D. Meng, B. Zheng, G. Lin and M. L. Sushko, *Commun. Comput. Phys.*, 2014, **16**, 1298–1322.